

Improved Point Estimation for the Rayleigh Regression Model

B. G. Palm*

F. M. Bayer[†]R. J. Cintra[‡]

Abstract

The Rayleigh regression model was recently proposed for modeling amplitude values of synthetic aperture radar (SAR) image pixels. However, inferences from such model are based on the maximum likelihood estimators, which can be biased for small signal lengths. The Rayleigh regression model for SAR images often takes into account small pixel windows, which may lead to inaccurate results. In this letter, we introduce bias-adjusted estimators tailored for the Rayleigh regression model based on: (i) the Cox and Snell's method; (ii) the Firth's scheme; and (iii) the parametric bootstrap method. We present numerical experiments considering synthetic and actual SAR data sets. The bias-adjusted estimators yield nearly unbiased estimates and accurate modeling results.

Keywords

Bias correction, Rayleigh regression model, SAR images, Small signal lengths inferences

1 Introduction

The classical linear regression model is widely employed to estimate an unknown and deterministic parameter vector assuming the Gaussian distribution [16]. However, practical contexts often exhibit non-Gaussian behavior. An alternative to the Gaussian model is provided by the Rayleigh distribution which is capable of characterizing asymmetric, continuous, and nonnegative signals, such as the amplitude values of synthetic aperture radar (SAR) image pixels [9, 15]. The Rayleigh regression model was proposed in [13], where a methodology for point estimation, large data record results, and goodness-of-fit measures were presented and discussed in the context of SAR image detection.

Parameter inference based on the Rayleigh regression model can be achieved by means of the maximum likelihood estimation, inheriting its good asymptotic properties for large signal lengths. However, if the signal length N is small, then the maximum likelihood estimators (MLE) present a bias in the order of N^{-1} , which can be regarded as problematic [3]. For instance, in [13], the detection of different land cover types in SAR images was performed based on pixel windows of more than 126 pixels. However, if smaller windows, such as 3×3 , are selected for Rayleigh regression model parameter estimation, then the obtained results can be severely biased.

An approach to address this issue is by means of inferential corrections [3]. Three widely bias-adjusted methods are the Cox and Snell's [4], Firth's [8], and parametric bootstrap [6] schemes. The Cox and Snell's method is an analytical approach used to obtain second order corrected estimators. The Firth's method is a preventive method [8] of bias reduction which modify the score function before obtaining parameter estimates based on the analytical second order biases of the MLE [8]. Finally, the bootstrap method is a computationally intensive method based on resampling, being suitable for inferential corrections when N is small [6].

To the best of our knowledge, the literature lacks bias-adjusted estimators for the parameters of the Rayleigh regression model. In this paper, our chief goal is to obtain accurate point estimation approaches to address this literature gap.

*Programa de Pós-graduação em Estatística, Universidade Federal Pernambuco and Department of Telecommunications, Aeronautics Institute of Technology (ITA), Brazil (E-mail: brunagpalm@gmail.com).

[†]Departamento de Estatística and LACESM, Universidade Federal de Santa Maria, Brazil (E-mail: bayer@ufsm.br).

[‡]Signal Processing Group, Departamento de Estatística, Universidade Federal Pernambuco, Brazil (E-mail: rjpsc@de.ufpe.br).

2 The Rayleigh Regression Model

The Rayleigh regression model was proposed in [13] and can be defined as follows. Let Y be a Rayleigh distributed random variable with mean parameter $\mu > 0$. The probability density function of the mean-based Rayleigh distribution is given by [13]

$$f_Y(y; \mu) = \frac{\pi y}{2\mu^2} \exp\left(-\frac{\pi y^2}{4\mu^2}\right), \quad (1)$$

where $y > 0$ is the observed signal value. The mean and variance of Y are given, respectively, by $E(Y) = \mu$ and $\text{Var}(Y) = \mu^2 \left(\frac{4}{\pi} - 1\right)$.

Let $Y[1], Y[2], \dots, Y[N]$ be independent random variables, where each $Y[n]$ assumes values $y[n]$ and follows the Rayleigh density in (1) with mean $\mu[n]$, $n = 1, 2, \dots, N$. The Rayleigh regression model is defined assuming that the mean of the observed output signal $Y[n]$ can be written as

$$\eta[n] = g(\mu[n]) = \sum_{i=1}^k \beta_i x_i[n], \quad n = 1, 2, \dots, N,$$

where $k < N$ is the number of covariates considered in the model, $\boldsymbol{\beta} = (\beta_1, \beta_2, \dots, \beta_k)^\top$ is the vector of unknown linear parameters, $\mathbf{x}[n] = (x_1[n], x_2[n], \dots, x_k[n])^\top$ is the vector of independent input variables, $g: \mathbb{R}^+ \rightarrow \mathbb{R}$ is a strictly monotonic and twice differentiable link function, and $\eta[n]$ is the linear predictor [13].

Parameter estimation can be performed using the maximum likelihood method, as discussed in [13]. The estimated vector $\hat{\boldsymbol{\beta}}$ is obtained by maximizing the logarithm of the likelihood function. The log-likelihood function of the parameter vector $\boldsymbol{\beta}$ for the observed signal is $\ell(\boldsymbol{\beta}) = \sum_{n=1}^N \ell_n(\mu[n])$, where $\ell_n(\mu[n]) = \log\left(\frac{\pi}{2}\right) + \log(y[n]) - \log(\mu[n]^2) - \frac{\pi y[n]^2}{4\mu[n]^2}$.

The score vector can be written as $U(\boldsymbol{\beta}) = \mathbf{X}^\top \cdot \mathbf{T} \cdot \mathbf{v}$, where \mathbf{X} is the $N \times k$ matrix whose n th row is $\mathbf{x}[n]^\top$, $\mathbf{T} = \text{diag}\left\{\frac{1}{g'(\mu[1])}, \frac{1}{g'(\mu[2])}, \dots, \frac{1}{g'(\mu[N])}\right\}$, and $\mathbf{v} = \left(\frac{\pi y[1]^2}{2\mu[1]^3} - \frac{2}{\mu[1]}, \frac{\pi y[2]^2}{2\mu[2]^3} - \frac{2}{\mu[2]}, \dots, \frac{\pi y[N]^2}{2\mu[N]^3} - \frac{2}{\mu[N]}\right)^\top$. Finally, the Fisher information matrix is given by $\mathbf{I}(\boldsymbol{\beta}) = \mathbf{X}^\top \cdot \mathbf{W} \cdot \mathbf{X}$, where $\mathbf{W} = \text{diag}\left\{\frac{4}{\mu[1]^2} \left(\frac{d\mu[1]}{d\eta[1]}\right)^2, \dots, \frac{4}{\mu[N]^2} \left(\frac{d\mu[N]}{d\eta[N]}\right)^2\right\}$. Further mathematical properties, including large data record results and optimization procedures, are detailed in [13].

3 Bias Correction of MLE

Generally, for small N , the MLE $\hat{\boldsymbol{\beta}}$ for $\boldsymbol{\beta}$ may be biased and the associated bias can be expressed as $B(\hat{\boldsymbol{\beta}}) = E[\hat{\boldsymbol{\beta}}] - \boldsymbol{\beta}$ [3]. The Cox and Snell's bias correction formula for the a th component of $\hat{\boldsymbol{\beta}}$ is given by

$$B(\hat{\beta}_a) = \sum_{r,s,u} \kappa^{ar} \kappa^{su} \left\{ \kappa_{rs}^{(u)} - \frac{1}{2} \kappa_{rsu} \right\}, \quad (2)$$

where $\kappa_{rs} = E\left(\frac{\partial^2 \ell}{\partial \beta_r \partial \beta_s}\right)$, $\kappa_{rs}^{(u)} = \frac{\partial \kappa_{rs}}{\partial \beta_u}$, $\kappa_{rsu} = E\left(\frac{\partial^3 \ell}{\partial \beta_r \partial \beta_s \partial \beta_u}\right)$, $-\kappa^{ar}$ and $-\kappa^{su}$ are the (a, r) and (s, u) elements of the inverse of the Fisher information matrix, respectively [4]. The cumulants obtained for the Rayleigh regression model can be found in the Appendix.

The second order bias of $\hat{\boldsymbol{\beta}}$ is defined as

$$B(\hat{\boldsymbol{\beta}}) = \mathbf{I}^{-1}(\hat{\boldsymbol{\beta}}) \cdot \mathbf{X}^\top \cdot \mathbf{W} \cdot \boldsymbol{\delta},$$

where $\boldsymbol{\delta}$ is the main diagonal of $\mathbf{X} \cdot \mathbf{I}^{-1}(\hat{\boldsymbol{\beta}}) \cdot \mathbf{X}^\top$ and $\mathbf{W} = \text{diag}\left[-\frac{2}{\mu[n]^3} \left(\frac{d\mu[n]}{d\eta[n]}\right)^3 - \frac{2}{\mu[n]^2} \left(\frac{d\mu[n]}{d\eta[n]}\right)^2 \cdot \frac{\partial}{\partial \mu[n]} \left(\frac{d\mu[n]}{d\eta[n]}\right)\right]$. Replacing the unknown parameters by their MLE, we have the MLE $\hat{B}(\hat{\boldsymbol{\beta}})$ for $B(\hat{\boldsymbol{\beta}})$, and bias-adjusted estimators can be derived removing $\hat{B}(\hat{\boldsymbol{\beta}})$ of $\hat{\boldsymbol{\beta}}$ [3]. Hence, corrected estimators based on the Cox and Snell's method, $\tilde{\boldsymbol{\beta}}$, are obtained as $\tilde{\boldsymbol{\beta}} = \hat{\boldsymbol{\beta}} - \hat{B}(\hat{\boldsymbol{\beta}})$ [4]. The Firth's method removes the second-order bias by modifying the original score function $U(\boldsymbol{\beta})$ according

Table 1: Results of the Monte Carlo simulation for point estimation of Scenarios 1 and 2. Best results are highlighted

		$\hat{\beta}_1$	$\tilde{\beta}_1$	$\hat{\beta}_1^*$	$\tilde{\beta}_1^*$	$\hat{\beta}_2$	$\tilde{\beta}_2$	$\hat{\beta}_2^*$	$\tilde{\beta}_2^*$	$\hat{\beta}_3$	$\tilde{\beta}_3$	$\hat{\beta}_3^*$	$\tilde{\beta}_3^*$
$N = 9$													
Scenario 1	RB(%)	-10.0546	0.9665	-0.4822	1.0152	-24.3255	-8.9817	-8.8812	-7.1089	-1.4237	1.0249	2.5234	1.2595
	RMSE	0.7083	0.7049	0.7068	0.7051	0.7960	0.7927	0.7924	0.7922	0.8083	0.8055	0.8087	0.8062
Scenario 2	RB(%)	-1.6082	-0.0595	-0.1941	-0.0252	-2.4411	-0.5491	0.2736	-0.4622	-	-	-	-
	RMSE	0.4625	0.4599	0.4610	0.4600	0.6979	0.6959	0.6980	0.6961	-	-	-	-
$N = 25$													
Scenario 1	RB(%)	-1.2113	1.1810	0.6506	1.4531	-13.9903	-4.1510	-2.1974	-4.5960	-1.8112	-0.3642	-0.0567	0.4670
	RMSE	0.3319	0.3317	0.3317	0.3316	0.3568	0.3562	0.3563	0.3565	0.3554	0.3548	0.3548	0.3549
Scenario 2	RB(%)	-0.2640	0.1544	0.1150	0.1812	-1.3497	-0.3138	-0.1566	-0.3695	-	-	-	-
	RMSE	0.2319	0.2318	0.2319	0.2319	0.3439	0.3432	0.3434	0.3432	-	-	-	-
$N = 49$													
Scenario 1	RB(%)	-0.9191	-0.0037	-0.1914	0.0997	-7.0768	-1.3383	-0.6904	-1.5395	-0.6448	0.2236	0.3203	0.1924
	RMSE	0.2226	0.2225	0.2225	0.2226	0.2381	0.2380	0.2380	0.2381	0.2365	0.2362	0.2362	0.2364
Scenario 2	RB(%)	-0.1297	0.0580	0.0462	0.0716	-0.7194	-0.1266	-0.0821	-0.1552	-	-	-	-
	RMSE	0.1588	0.1588	0.1588	0.1589	0.2306	0.2304	0.2304	0.2305	-	-	-	-

to $U^*(\beta) = U(\beta) - \mathbf{I}(\beta) \cdot B(\hat{\beta})$ [8], where $B(\hat{\beta})$ is the second-order bias computed in (2). The roots of the modified score function $U^*(\beta)$ constitute the corrected estimator $\hat{\beta}^*$ according to the Firth's method. In the bootstrap bias correction method, the bias estimation $\hat{B}(\hat{\beta})$ is numerically obtained through Monte Carlo simulations. A bootstrap estimate of the bias can be obtained by $\hat{B}_{\text{boot}}(\hat{\beta}) = \tilde{\beta}^* - \hat{\beta}$, where $\tilde{\beta}^* = \frac{1}{R} \sum_{b=1}^R \hat{\beta}_b$, R is the number of bootstrap replications, and $\hat{\beta}_b$ is the estimated values of β in each bootstrap replication. Thus, the corrected estimator based on the bootstrap method is given by $\hat{\beta}^* = \hat{\beta} - \hat{B}_{\text{boot}}(\hat{\beta}) = \hat{\beta} - (\tilde{\beta}^* - \hat{\beta}) = 2\hat{\beta} - \tilde{\beta}^*$ [6]. The above described bias-adjusted estimators share the same asymptotic properties with the usual MLE but are less biased for small N [7].

4 Numerical Experiments

4.1 Synthetic Data Modeling

Monte Carlo simulations were employed to evaluate the original MLE performance of the Rayleigh regression model parameters and their bias-adjusted versions. Synthetic SAR data was generated under two scenarios. Each scenario aimed at capturing asymmetric distributions. For Scenario 1, we selected the following parameters values: $\beta_1 = 0.5$, $\beta_2 = 0.5$, $\beta_3 = 1$, and covariates generated from the binomial distribution; whereas, for Scenario 2, we adopted $\beta_1 = 2.5$, $\beta_2 = 1.5$, and covariates generated from the Rayleigh distribution. We have for Scenarios 1 and 2, skewness about 4 and 3, respectively. The covariates values were kept constant for all Monte Carlo replications and the log link function was employed. The number of Monte Carlo and bootstrap replications were set equal to 5,000 and 1,000, respectively, and the signal lengths considered were $N \in \{9; 25; 49\}$. Such blocklengths are popular choices of window sizes in SAR image processing [1, 10, 14].

The percentage relative bias (RB%) and the root mean squared error (RMSE) were adopted as figures of merit to numerically evaluate the point estimators. Table 1 presents the simulation results for point estimation of the Rayleigh regression model parameters for Scenarios 1 and 2. We notice that the MLE can be strongly biased for small N . For instance, for Scenario 1 and $N = 9$, the relative biases of the MLE are approximately (in absolute values) 10%, 24%, and 1% for $\hat{\beta}_1$, $\hat{\beta}_2$, and $\hat{\beta}_3$, respectively. For this same signal length, the relative bias of $\tilde{\beta}_2$, $\hat{\beta}_2^*$, and $\tilde{\beta}_2^*$ are (in absolute values) 9%, 9%, and 7%, respectively. In general, the bias-corrected estimators present values closer to the true parameters when compared to the MLE and have similar performance in terms of relative bias and RMSE.

To evaluate the overall performances of the four estimators for each value of N , we employed the integrated relative

Table 2: Integrated relative bias squared norm results. Best results are highlighted

		MLE	Cox and Snell	Firth	Bootstrap
Scenario 1	$N = 9$	15.2190	5.2490	5.3378	2.8764
	$N = 25$	8.1747	2.5005	1.3235	2.7960
	$N = 49$	4.1369	0.7834	0.4531	1.0368
Scenario 2	$N = 9$	2.0670	0.3905	0.2372	0.2910
	$N = 25$	0.9725	0.2473	0.1374	0.2910
	$N = 49$	0.5169	0.0985	0.0666	0.1209

Table 3: Fitted models for San Francisco and CARABAS II SAR images

		$\hat{\beta}_1$	$\hat{\beta}_2$	$\hat{\beta}_1^*$	$\hat{\beta}_2^*$
SF — HH ~ HV	3×3	-2.9162	0.3091	-2.9318	3.6062
	7×7	-2.8978	0.0643	-2.9115	1.2344
SF — VV ~ HV	3×3	-2.2259	-0.1947	-2.1421	-1.3629
	7×7	-2.1621	0.0101	-2.1559	0.1569
CARABAS II	3×3	-1.9124	-0.4279	-1.7851	-1.2194
	7×7	-1.9896	0.1616	-1.9886	0.2314

bias squared norm (IRBSN) figure of merit [5], which is defined as $IRBSN = \sqrt{\frac{1}{k} \sum_{i=1}^k RB(\hat{\beta}_i)^2}$, where $RB(\hat{\beta}_i)$, $i = 1, 2, \dots, k$, corresponds to the values of RB% of each estimator. The values of IRBSN for Scenarios 1 and 2 are given in Table 2. The corrected estimators excel in terms of IRBSN. Additionally, among the evaluated estimators, the ones obtained by the Firth’s method present the smallest values of IRBSN in five of the six evaluated scenarios.

4.2 SAR Image Modeling

In this section, we present image modeling experiments considering two actual SAR data sets. For such, we considered (i) the San Francisco Bay (SF) associated to horizontal (HH), vertical (VV), and HV polarization channels SAR images; and (ii) an image obtained from CARABAS II, a Swedish ultrawideband (UWB) very-high frequency (VHF) SAR system. More details about these data sets can be found in [2, 11].

As the correlation between different channels has been considered as a scheme for detection of man-made targets and land cover classification in SAR imagery [17], we used the HV channel to describe the mean of the amplitude values of HH and VV channels—the resulted models are referred to as HH ~ HV and VV ~ HV, respectively. Additionally, San Francisco HV associated image is well correlated with the HH and VV channels: 0.8268 and 0.7593, respectively. To specify the mean of the amplitude values of the CARABAS II SAR image associated to mission one and pass one, we fitted the regression model considering as a covariate, an image with the same flight pass of the evaluated CARABAS II image (mission two and pass one)—the correlation value between both images is 0.4719. As the Rayleigh distribution is suitable for representing homogeneous areas [12], such as the sea/water ground type [2], we selected windows of 3×3 and 7×7 pixels related to the water area to fit the models.

The adjusted model results can be found in Table 3. We notice that the MLE and Firth-based estimators present different estimate values in all evaluated scenarios. For instance, considering the window of 7×7 pixels in the HH ~ HV model, $\hat{\beta}_2^*$ shows a value about 1820% bigger than $\hat{\beta}_2$. To quantify the performance of considered fitted models, we employed the estimated root mean square error measure computed between $y[n]$ and $\hat{\mu}[n]$ —here referred to as \widehat{RMSE} . For comparison purposes, we also fitted the standard Gaussian regression model—widely employed in signal modeling—and the Rayleigh distribution. The \widehat{RMSE} values for the considered models are given in Table 4; for all evaluated models, the Firth-based estimators present smaller values of \widehat{RMSE} .

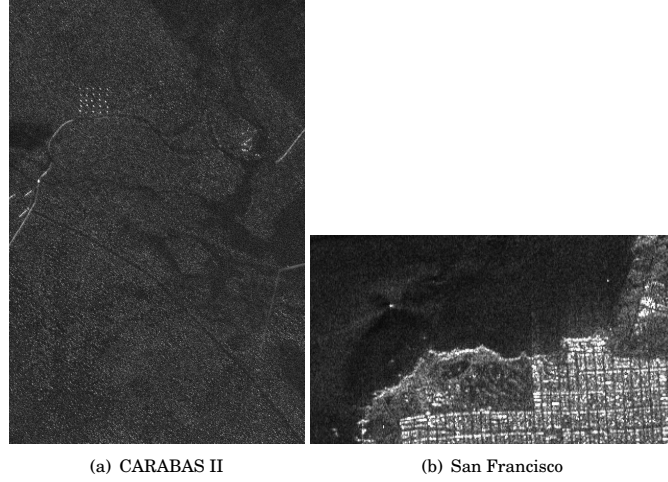


Figure 1: San Francisco and CARABAS II SAR images associated to HH polarization channel.

Table 4: Estimated root mean square error measure of the fitted models for San Francisco and CARABAS II SAR images. Best results are highlighted

		Firth-based Rayleigh regression	MLE-based Rayleigh regression	Gaussian regression	Rayleigh distribution
SF — HH ~ HV	3 × 3	0.0123	0.0133	1.0019	0.5662
	7 × 7	0.0157	0.0159	1.0020	0.5606
SF — VV ~ HV	3 × 3	0.0194	0.0222	1.0077	0.5085
	7 × 7	0.0326	0.0330	1.0088	0.4955
CARABAS II	3 × 3	0.0267	0.0296	1.0136	0.4730
	7 × 7	0.0427	0.0430	1.0130	0.4774

5 Conclusions

This letter introduced bias-adjusted estimators for the Rayleigh regression model parameters. We employed the Cox and Snell's, Firth's, and parametric bootstrap methods to obtain corrected estimators. Monte Carlo simulation results show that the discussed bias-adjusted estimators outperformed MLE in terms of relative bias and root mean square error; being the estimators based on the Firth's method the best performing approach. Additionally, the Firth-based estimators resulted in more accurate modeling results in the evaluated SAR images experiments than the ones presented by the MLE method, the Rayleigh distribution, and the Gaussian-based regression model. In conclusion, we recommend the use of corrected estimators based on the Firth's method to fit the Rayleigh regression model for small signal lengths.

Appendix

In this appendix, we present the cumulants of second and third order used to derive the Cox and Snell's and Firth's corrected estimators. From [13], we have that $\frac{d\ell_n(\mu[n])}{d\mu[n]} = \frac{\pi y[n]^2}{2\mu[n]^3} - \frac{2}{\mu[n]}, \frac{d\mu[n]}{d\eta[n]} = \frac{1}{g'(\mu[n])}, \frac{\partial\eta[n]}{\partial\beta_i} = x_i[n], \frac{\partial^2\ell_n(\mu[n])}{\partial\mu[n]^2} = \frac{2}{\mu[n]^2} - \frac{3\pi y[n]^2}{2\mu[n]^4}$, and $E\left[\frac{d^2\ell_n(\mu[n])}{d\mu[n]^2}\right] = -\frac{4}{\mu[n]^2}$. Note that $\frac{\partial^3\ell_n(\mu[n])}{\partial\mu[n]^3} = \frac{d}{d\mu[n]}\left(\frac{\partial^2\ell_n(\mu[n])}{\partial\mu[n]^2}\right) = \frac{6\pi y[n]^2}{\mu[n]^5} - \frac{4}{\mu[n]^3}$. Taking the expected value of the derivative above, we have $E\left(\frac{\partial^3\ell_n(\mu[n])}{\partial\mu[n]^3}\right) = \frac{24}{\mu[n]^3} - \frac{4}{\mu[n]^3} = \frac{20}{\mu[n]^3}$. From [13], the second order cumulant is given by $\kappa_{rs} = E\left[\frac{\partial^2\ell(\beta)}{\partial\beta_r\partial\beta_s}\right] = \sum_{n=1}^N \left[-\frac{4}{\mu[n]^2} \left(\frac{d\mu[n]}{d\eta[n]}\right)^2 x_s[n]x_r[n]\right]$. Differentiating the second order cumulant with respect β_u , we obtain $\kappa_{rs}^{(u)}$ as $\frac{\partial\kappa_{rs}}{\partial\beta_u} = \sum_{n=1}^N \left[\frac{8}{\mu[n]^3} \left(\frac{d\mu[n]}{d\eta[n]}\right)^3 - \frac{8}{\mu[n]^2} \left(\frac{d\mu[n]}{d\eta[n]}\right)^2 \frac{\partial}{\partial\mu[n]}\left(\frac{d\mu[n]}{d\eta[n]}\right)\right] x_u[n]x_s[n]x_r[n]$. The third order derivatives of the log-likelihood function is

$$\begin{aligned} \frac{\partial^3\ell(\beta)}{\partial\beta_r\partial\beta_s\partial\beta_u} &= \sum_{n=1}^N \left[\frac{\partial^3\ell_n(\mu[n])}{\partial\mu[n]^3} \left(\frac{d\mu[n]}{d\eta[n]}\right)^2 + \frac{\partial}{\partial\mu[n]} \right. \\ &\cdot \left. \left(\frac{d\mu[n]}{d\eta[n]}\right)^2 \frac{\partial^2\ell_n(\mu[n])}{\partial\mu[n]^2} + \frac{\partial^2\ell_n(\mu[n])}{\partial\mu[n]^2} \frac{d\mu[n]}{d\eta[n]} \frac{\partial}{\partial\mu[n]}\left(\frac{d\mu[n]}{d\eta[n]}\right) \right. \\ &\left. + \frac{\partial}{\partial\mu[n]} \left(\frac{d\mu[n]}{d\eta[n]} \frac{\partial}{\partial\mu[n]} \frac{d\mu[n]}{d\eta[n]}\right) \frac{d\ell_n(\mu[n])}{d\mu[n]} \right] \frac{d\mu[n]}{d\eta[n]} x_u[n]x_r[n]x_s[n]. \end{aligned}$$

Taking the expected value, we obtain the third order cumulant

$$\kappa_{rsu} = \sum_{n=1}^N \left[\frac{20}{\mu[n]^3} \left(\frac{d\mu[n]}{d\eta[n]}\right)^3 - \frac{12}{\mu[n]^2} \left(\frac{d\mu[n]}{d\eta[n]}\right)^2 \frac{\partial}{\partial\mu[n]}\left(\frac{d\mu[n]}{d\eta[n]}\right) \right] x_u[n]x_r[n]x_s[n].$$

From the above expressions, we have that $\kappa_{rs}^{(u)} - \frac{1}{2}\kappa_{rsu} = \sum_{n=1}^N \left[-\frac{2}{\mu[n]^3} \left(\frac{d\mu[n]}{d\eta[n]}\right)^3 - \frac{2}{\mu[n]^2} \left(\frac{d\mu[n]}{d\eta[n]}\right)^2 \frac{\partial}{\partial\mu[n]}\left(\frac{d\mu[n]}{d\eta[n]}\right) \right] x_u[n]x_s[n]x_r[n]$.

Now, it is possible to compute the second order biases of the Rayleigh regression model MLE as $\sum_{r,s,u} \kappa^{ar} \kappa^{su} \left\{ \kappa_{rs}^{(u)} - \frac{1}{2}\kappa_{rsu} \right\} = \sum_{n=1}^N w[n] \sum_r \kappa^{ar} x_r[n] \sum_{s,u} x_s[n] \kappa^{su} x_u[n]$, where $w[n] = -\frac{2}{\mu[n]^3} \left(\frac{d\mu[n]}{d\eta[n]}\right)^3 - \frac{2}{\mu[n]^2} \left(\frac{d\mu[n]}{d\eta[n]}\right)^2 \frac{\partial}{\partial\mu[n]}\left(\frac{d\mu[n]}{d\eta[n]}\right)$. Note that $\sum_{n=1}^N w[n] \sum_r \kappa^{ar} x_r[n] \sum_{s,u} x_s[n] \kappa^{su} x_u[n] = e_a^\top \mathbf{I}^{-1}(\beta) \sum_{n=1}^N w[n] x[n] (x^\top[n] \mathbf{I}^{-1}(\beta) x[n])$, where e_a is defined as the a th column vector of the $k \times k$ identity matrix. Then, $\sum_{r,s,u} \kappa^{ar} \kappa^{su} \left\{ \kappa_{rs}^{(u)} - \frac{1}{2}\kappa_{rsu} \right\} = e_a^\top \cdot \mathbf{I}^{-1}(\beta) \cdot \mathbf{X}^\top \cdot \mathbf{W} \cdot \delta$.

References

- [1] D. I. ALVES, B. G. PALM, M. I. PETERSSON, V. T. VU, R. MACHADO, B. F. UCHOA-FILHO, P. DAMMERT, AND H. HELLSTEN, *A statistical analysis for wavelength-resolution SAR image stacks*, IEEE Geoscience and Remote Sensing Letters, 17 (2019), pp. 227–231.

- [2] R. J. CINTRA, A. C. FRERY, AND A. D. NASCIMENTO, *Parametric and nonparametric tests for speckled imagery*, Pattern Analysis and Applications, 16 (2013), pp. 141–161.
- [3] G. M. CORDEIRO AND F. CRIBARI-NETO, *An Introduction to Bartlett Correction and Bias Reduction*, Springer, 2014.
- [4] D. R. COX AND E. J. SNELL, *A general definition of residuals*, Journal of the Royal Statistical Society: Series B (Methodological), 30 (1968), pp. 248–265.
- [5] F. CRIBARI-NETO AND K. L. VASCONCELLOS, *Nearly unbiased maximum likelihood estimation for the beta distribution*, Journal of Statistical Computation and Simulation, 72 (2002), pp. 107–118.
- [6] B. EFRON, *Bootstrap methods: Another look at the jackknife*, The Annals of Statistics, 7 (1979), pp. 1–26.
- [7] B. EFRON AND R. J. TIBSHIRANI, *An Introduction to the Bootstrap*, Monographs on Statistics and Applied Probability 57, 1994.
- [8] D. FIRTH, *Bias reduction of maximum likelihood estimates*, Biometrika, 80 (1993), pp. 27–38.
- [9] N. R. GOMES, P. DAMMERT, M. I. PETERSSON, V. T. VU, AND H. HELLSTEN, *Comparison of the Rayleigh and k -distributions for application in incoherent change detection*, IEEE Geoscience and Remote Sensing Letters, 16 (2018), pp. 756–760.
- [10] G.-T. LI, C.-L. WANG, P.-P. HUANG, AND W.-D. YU, *SAR image despeckling using a space-domain filter with alterable window*, IEEE Geoscience and Remote Sensing Letters, 10 (2012), pp. 263–267.
- [11] M. LUNDBERG, L. M. H. ULANDER, W. E. PIERSON, AND A. GUSTAVSSON, *A challenge problem for detection of targets in foliage*, in Proc. SPIE, vol. 6237, 2006.
- [12] C. OLIVER AND S. QUEGAN, *Understanding synthetic aperture radar images*, SciTech Publishing, 2004.
- [13] B. G. PALM, F. M. BAYER, R. J. CINTRA, M. I. PETERSSON, AND R. MACHADO, *Rayleigh regression model for ground type detection in SAR imagery*, IEEE Geoscience and Remote Sensing Letters, 16 (2019), pp. 1660–1664.
- [14] J.-M. PARK, W.-J. SONG, AND W. PEARLMAN, *Speckle filtering of SAR images based on adaptive windowing*, IEE Proceedings–Vision, Image and Signal Processing, 146 (1999), pp. 191–197.
- [15] M. N. SUMAIYA AND R. S. S. KUMARI, *Unsupervised change detection of flood affected areas in SAR images using Rayleigh-based Bayesian thresholding*, IET Radar, Sonar & Navigation, 12 (2018), pp. 515–522.
- [16] A. WIESEL, Y. C. ELDAR, AND A. YEREDOR, *Linear regression with Gaussian model uncertainty: Algorithms and bounds*, IEEE Transactions on Signal Processing, 56 (2008), pp. 2194–2205.
- [17] D. XIANG, T. TANG, C. HU, Q. FAN, AND Y. SU, *Built-up area extraction from PolSAR imagery with model-based decomposition and polarimetric coherence*, Remote Sensing, 8 (2016), p. 685.